ELSEVIER

Journal of Power Sources 65 (1997) 121–128

JOURNAL OF POWER SOURCES

19

Development of an equivalent-circuit model for the lithium/iodine battery

Craig L. Schmidt *, Paul M. Skarstad

Medtronic Inc., 6700 Shingle Creek Parkway, Minneapolis, MN 55430, USA

Received 4 November 1996; accepted 19 November 1996

Abstract

The lithium/iodine battery is the most widely used power source for implantable cardiac pacemakers. While the average power demands of pacemakers are very low, the instantaneous power requirements can challenge the capabilities of this high impedance battery. Thus, there is a need to predict the transient-response behavior of new battery designs. Impedance spectroscopy was used to characterize the behavior of a variety of cell designs as a function of cell design, depth-of-discharge, and current density. An equivalent-circuit model was developed in terms of the physical elements which contribute to electrical resistance, capacitance, and electrochemical polarization. The transient-response predicted by this simple equivalent-circuit model was compared to pulse data from actual batteries and found to be in excellent agreement.

Keywords: Lithium primary batteries/iodine; Mathematical modelling

1. Introduction

The lithium/iodine battery has been used as a power source for implantable cardiac pacemakers for over twenty years. Its high reliability and low self-discharge rate make it ideally suited for this application. As a result, virtually all cardiac pacemakers today are powered by the lithium/iodine battery.

The lithium/iodine battery is also characterized by very high internal impedance which increases throughout discharge. Its characteristic knee-shaped discharge curve results primarily from the corresponding *IR* losses. In the past, the power requirements for cardiac pacemakers were very low (around 50 μW) and the high internal impedance of the cells was not a significant factor in determining the useful life of the battery. Nearly all of the available iodine was consumed by the time the load voltage dropped to unacceptable levels.

While the average power requirements of cardiac pacemakers have tended to decrease, the instantaneous power demands have grown substantially due to the incorporation of more complex electronic circuits, new features, and new therapies. As the instantaneous power demands increase, it is possible to drive the battery voltage prematurely to unacceptably low levels. If the transient-response characteristics of the battery are well understood, many of these high-power features can be implemented through careful power management. In general, this requires that the battery be described in terms of an equivalent-circuit model and that such a circuit can be predicted as a function of discharge depth prior to the development of a new battery design.

Previously we have described in general terms the development of three types of models used to characterize implantable medical batteries [1]. We have described in detail the development of a model which allows the discharge characteristics of a new cell design to be accurately predicted [2–4]. This model relates the physical elements of the battery design to the electrical resistance and electrochemical polarization observed during constant-current discharge. It was the goal of the present work to extend the model to predict transient-response behavior.

2. Background

For the sake of continuity and clarity a brief review of the major sources of voltage loss in the lithium/iodine battery is repeated here. Details of the lithium/iodine battery design and other characteristics can be found elsewhere [5–7].

The voltage losses observed during discharge of a lithium/iodine battery can be conveniently categorized as ohmic losses, non-ohmic polarization, and loss of open-circuit potential. The ohmic (current independent) losses are dominated by the electrolyte resistance (i.e., lithium iodide for-

* Corresponding author.

PII S0378-7753(96)02604-3

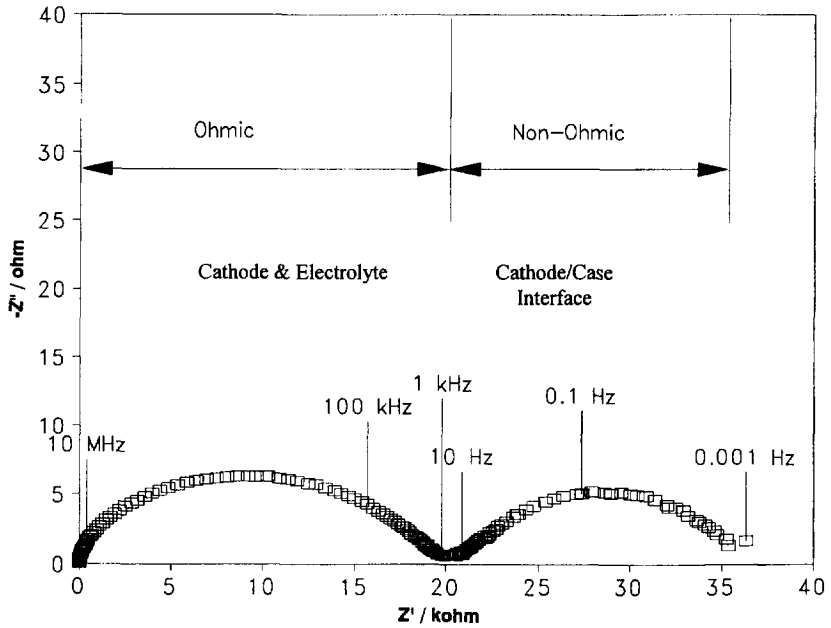

Fig. 1. Typical impedance spectrum of a lithium/iodine battery presented in the complex-plane.

mation) during the first 70% to 80% of discharge. The cathode, which is a two-phase material consisting of crystalline iodine and an iodine/poly-2-vinyl pyridine complex, provides a relatively minor contribution to the ohmic resistance as long as the crystalline iodine is available to saturate the liquid phase. After the crystalline iodine is depleted, the cathode resistance grows exponentially and, depending on cell design, may eventually dominate the total ohmic resistance.

The non-ohmic (current dependent) resistance arises primarily at the cathode/current collector interface [2]. It should be noted that the stainless steel battery case serves as the current collector in our cell designs. The non-ohmic resistance measured by impedance spectroscopy exhibits a current dependence consistent with a charge transfer resistance. In addition, a part of the non-ohmic polarization is related to concentration polarization within the cathode. When the cathode composition is in the two-phase region (i.e., crystalline iodine is still available), the non-ohmic polarization remains relatively constant. As the cathode becomes depleted of iodine, the non-ohmic polarization increases rapidly and is comparable in magnitude to the ohmic losses.

The open-circuit voltage of the lithium/iodine battery is constant as long as the cathode composition is in the two-phase region. After depletion of the crystalline iodine, the open-circuit voltage decreases as the cathode is further discharged. The total loss of open-circuit voltage is typically less than 30 mV at the point at which the load voltage falls to unacceptable levels. Thus the loss of open-circuit voltage represents the least significant source of voltage loss in a practical lithium/iodine battery.

Fig. 1 shows a typical impedance spectrum of a lithium/iodine battery in which the ohmic and non-ohmic contributions to the cell impedance are noted.

3. Experimental

The batteries used in these studies were hermetically sealed, central anode designs [5]. Nine separate battery designs were studied having capacities ranging from about 0.60 to about 1.7 Ah. Discharge current densities ranged from about 2 to about 10 mA cm^{-2}. Impedance spectra were collected with a Solartron 1255 frequency response analyzer interfaced to an EG&G PAR 273a potentiostat. Typically, the cells remained on load during the measurement of impedance data.

4. Results and discussion

As is typical of electrochemical systems, the complex-plane plots contain somewhat flattened semi-circles (see Fig. 1) and cannot be perfectly represented by a pure resistor and capacitor in parallel. For our purposes, however, it was necessary to approximate the impedance behavior using ideal circuit elements. This allows the battery behaviour to be simulated through commercially available circuit simulation software or to be approximated with the use of a power supply and a collection of resistors and capacitors. These approaches allow system simulations and bench tests to be completed prior to finalization of circuit and battery design. Our approach was to use the intersections of an arc with the real axis to define the resistance value and to calculate the capacitance as:

$$C = \frac{1}{\omega_{max} R}$$

where ω_{max} is the angular frequency at the apex of the arc.

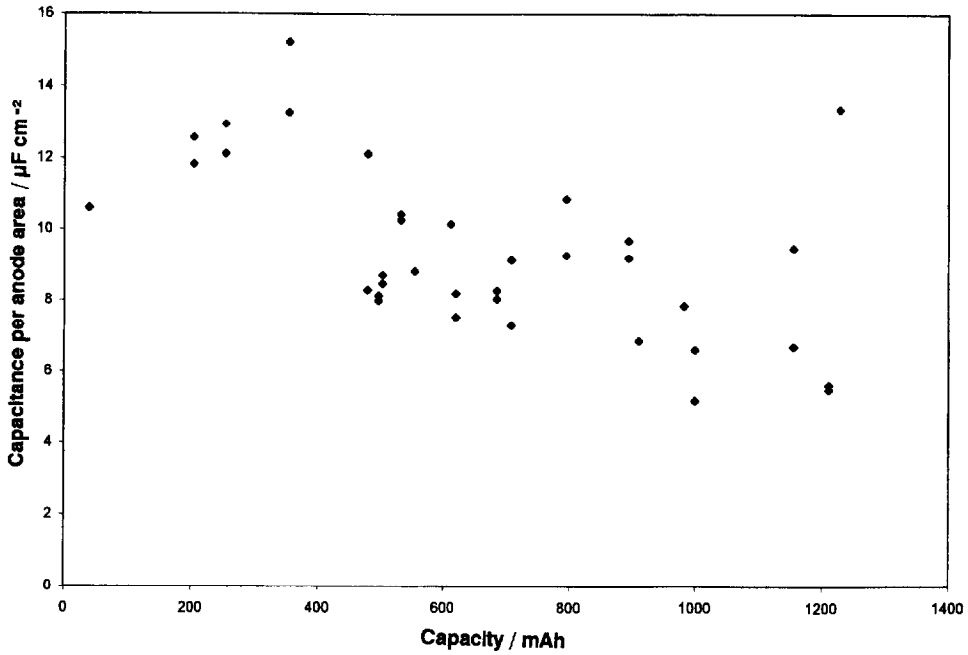

Fig. 2. Double-layer capacitance (normalized for anode area) as a function of discharged capacity for a single battery design.

The effect of approximating the impedance behavior in this manner will be discussed later.

4.1. Double-layer capacitance

As mentioned in Section 2, the non-ohmic impedance has been shown to be consistent with a charge-transfer resistance residing at the cathode/case interface. Thus it would be expected that the corresponding capacitance represents a double-layer capacitance. Furthermore, it might be expected that the double-layer capacitance would be relatively independent of cathode composition and, hence, independent of discharge depth.

Fig. 2 shows the measured capacitance associated with the charge transfer resistance for a given cell design as a function of depth of discharge. These data represent approximately 40 cells discharged at current densities ranging from 2 to 5 mA cm^{-2}. The measured capacitance is normalized by the anode area under the assumption that the close proximity of the anode to the case would tend to localize the current density to this area.

The average value of the area normalized capacitance is around 10 $\mu F\ cm^{-2}$. This is a reasonable value for a double-layer capacitance and provides support for this hypothesis. Although it is not apparent from the data as presented in Fig. 2, there is no correlation between the measured capacitance and the discharge rate. The scatter in the data represents normal cell-to-cell variation. There does, however, appear to be some decrease in the measured capacitance at greater depths of discharge. A similar trend was observed for every cell design included in this study, except that the cells with less capacity exhibited steeper slopes.

Fig. 3(a)–(d) shows the double-layer capacitance of several cell designs plotted as a function of depth-of-discharge instead of capacity. These cells were of a similar design in that they were the same thickness and width and differed only in the height dimension. The anode area and capacity of each cell is given in the legend. The capacitance was again normalized by the anode area. As in Fig. 2, there is significant scatter in the data representing typical cell-to-cell variation. However, each plot yields similar area normalized capacitance values and a similar downward trend in capacitance with depth-of-discharge. Nearly identical results were obtained with all cell designs included in this study.

One possible explanation for this behavior may be that the normalization of the double-layer capacitance by the anode area may not be strictly correct. Because the current densities are low and the interfacial resistance is high, the effective area of the cathode/case interface may be significantly greater than the area of the adjacent anode. The total cathode/case interfacial area exceeds the anode area by a factor of 1.7 to 2.4 depending on cell design. As the cathode is discharged, its volume decreases and the remaining cathode becomes located immediately over the anode. By the time discharge of the cathode is nearly complete, the area around the edges of the anode are completely devoid of cathode. Thus it may be more appropriate to normalize the double-layer capacitance by the entire cathode/case interfacial area at the beginning of discharge and by the anode area at the end of discharge. This would result in an decrease in capacitance by a factor of 1.7 to 2.4 between the beginning and end of discharge. This agrees approximately with the observation in Fig. 3(a)–(d).

4.2. Geometric capacitance

The remaining capacitance can be assigned to the geometric capacitance between the central lithium anode and the

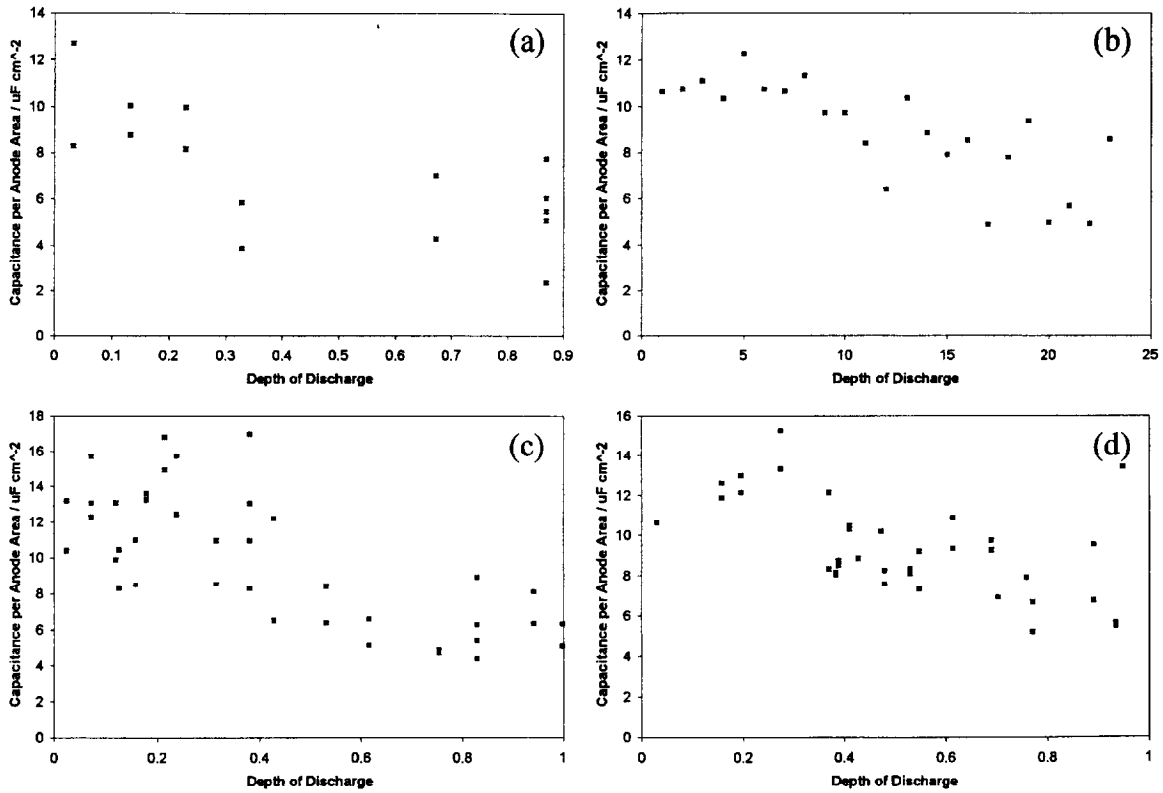

Fig. 3. Double-layer capacitance (normalized for anode area) as a function of depth-of-discharge for several battery designs differing in one dimension. Anode areas and cathode capacities are: (a) 3.8 cm^2, 610 mAh; (b) 5.6 cm^2, 830 mAh; (c) 7.3 cm^2, 1000 mAh; (d) 10.8 cm^2, 1300 mAh.

battery case. Fig. 4 shows how the geometric capacitance varies throughout discharge for a typical cell design. Note that the magnitude of the geometric capacitance decreases by about two orders of magnitude from the beginning to end of discharge.

There are at least two factors which contribute to the decreasing value of the geometric capacitance. First, as the lithium anode is consumed, the anode-to-case spacing increases by a factor of about three. Second, the composition of the dielectric material changes radically. At the beginning

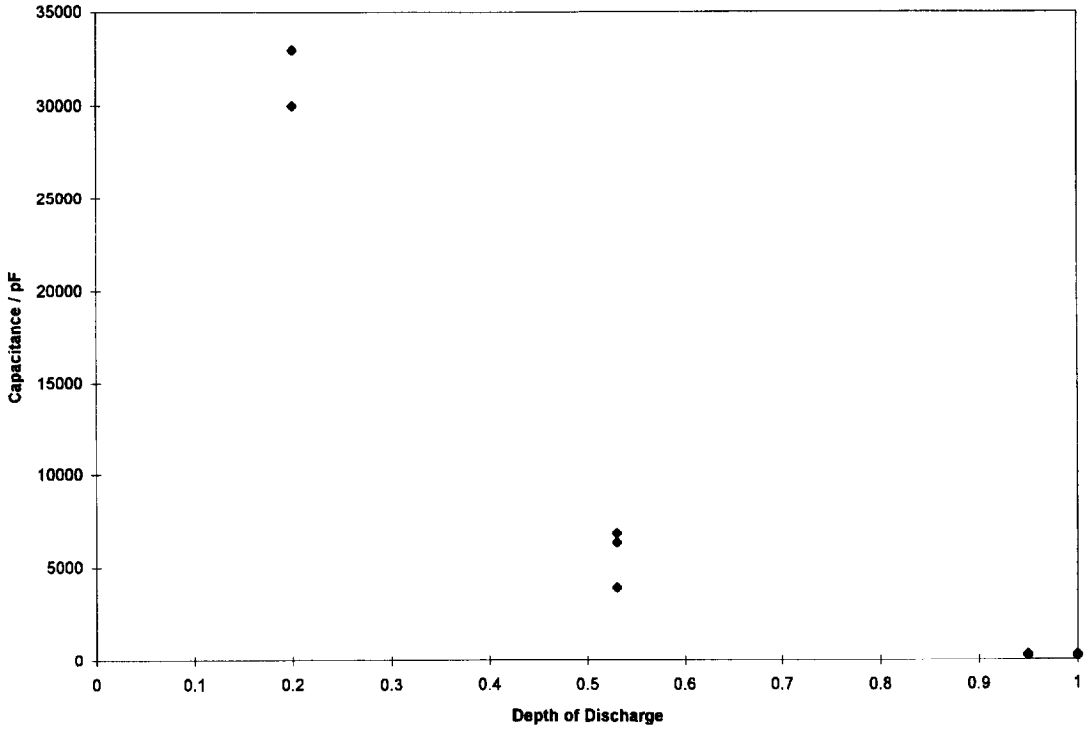

Fig. 4. Geometric capacitance as a function of discharged capacity for a typical cell design.

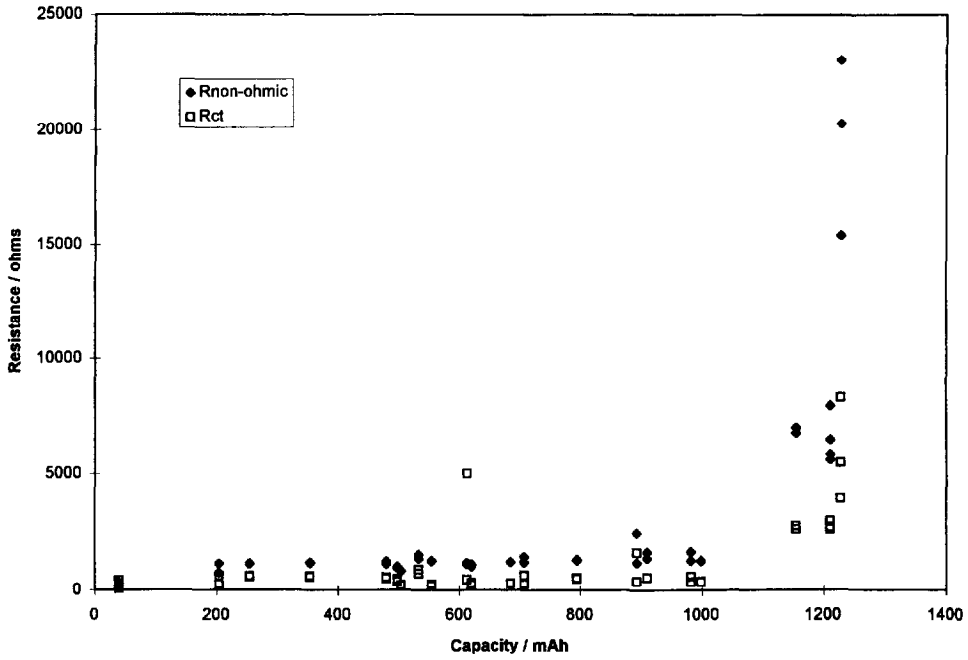

Fig. 5. Charge-transfer resistance and total non-ohmic polarization as a function of discharged capacity for a typical cell design.

of discharge, the dielectric material consists of a very thin film of lithium iodide and a much thicker layer of the cathode material.

By the end of discharge, the inter-electrode space is filled almost entirely by lithium iodide. While we have not measured the dielectric constant of the cathode material, we expect it to be much higher than that of lithium iodide.

We have collected much less data for the geometric capacitance than for the double-layer capacitance. One reason for this is that the time constant for the geometric capacitance and ohmic resistance is small enough that the effect of the geometric capacitance only becomes relevant at frequencies above about 10 000 Hz. In most of our applications, we are not interested in the transient-response of the battery at these high frequencies. The second reason for our limited data in this area is that the collection of accurate high frequency data requires extreme care and precludes the use of a potentiostat. This process is cumbersome and has been avoided wherever possible.

Our approach for modelling the geometric capacitance, when needed, has been to fit an empirical function to the limited data and then scale the data by the anode area.

4.3. Ohmic resistance

As described earlier, the ohmic resistance is determined by the electrolyte resistance and cathode resistance. It is not possible to resolve these two components by impedance spectroscopy at any depth-of-discharge. A description of the functional forms used to model the ohmic resistance can be found in Ref. [4] and will not be discussed further here.

4.4. Non-ohmic polarization

In our previous work, we modelled the entire non-ohmic polarization with a single function which incorporated loss of open-circuit potential, concentration polarization, and activation overpotential. This was a useful approach for predicting the load voltage of the battery under constant current discharge conditions. It is not useful, however, for predicting transient-response characteristics since each of these contributions has a drastically different time dependence.

As discussed earlier, the open-circuit voltage is constant throughout most of discharge and amounts to no more than about 30 mV at the end of discharge. The remainder of the non-ohmic polarization is defined by:

$$\eta_{\text{conc}} + \eta_{\text{act}} = V_{\text{oc}} - IR_{\text{ohmic}}$$

or by:

$$R_{\text{non-ohmic}} = R_{\text{conc}} + R_{\text{ct}} = R_{\text{dc}} - R_{\text{ohmic}}$$

Both the ohmic resistance, R_{ohmic}, and the charge-transfer resistance, R_{ct}, are measurable by impedance spectroscopy as shown in Fig. 1. The d.c. resistance, R_{dc}, is calculated from the load voltage and the concentration polarization, expressed as either η_{conc} or R_{conc}, is calculated by difference.

Fig. 5 compares the charge transfer resistance to the total non-polarization as a function of discharged capacity for a typical cell design. As expected from our previous work, both quantities remain relatively constant until the cathode reaches its single-phase composition. Then both quantities increase rapidly as the iodine activity decreases.

The most surprising result of this study is shown in Fig. 6. Here the ratio $R_{\text{ct}}/R_{\text{non-ohmic}}$ is plotted versus discharged capacity for a typical cell design. This particular plot repre-

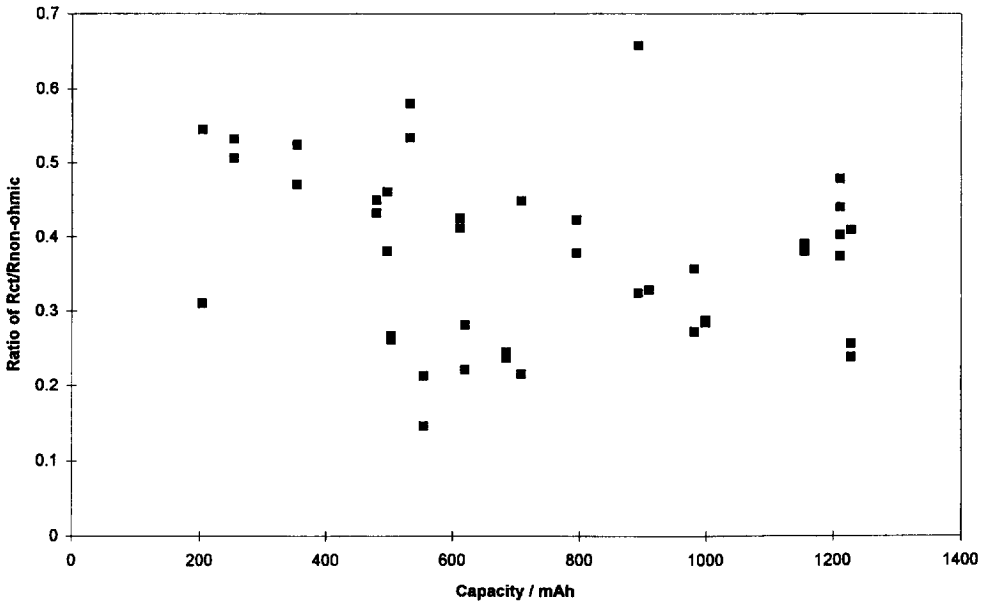

Fig. 6. Ratio of charge-transfer resistance to total non-ohmic polarization as a function of discharged capacity for a typical cell design.

sents the same set of batteries used to create Fig. 2. Note that the impedance data were collected over a range of current densities. Although there is a good deal of cell-to-cell variation, the ratio $R_{ct}/R_{non\text{-}ohmic}$ is essentially independent of current and cathode composition. The average value of the ratio is about 0.45. We have observed nearly identical behavior and a similar ratio for all of the cells designs included in this study.

It is not surprising that both R_{ct} and R_{conc} increase with decreasing iodine activity or that both decrease with increasing current density (as long as the current density is far below its mass transport limit). Conversely, it is very surprising that the ratio remains so constant over such a wide range of current density, cathode composition and cell design. Although we do not fully understand this phenomenon, this simple relationship allows a convenient means to estimate the charge transfer resistance from the total non-ohmic resistance as calculated from the function in Ref. [4].

4.5. Equivalent-circuit model

Fig. 7 shows an approximate equivalent-circuit model for the lithium/iodine battery which summarizes all of the components described above. Note that we have chosen to represent the concentration polarization, η_{conc}, as voltage source opposed to the open-circuit voltage, V_{oc}. The time constant for the development of concentration polarization is of the order of minutes to hours. Thus, while it is a significant contributor to the voltage loss observed during a constant current discharge, it can be treated as a time-independent voltage loss on a short time scale.

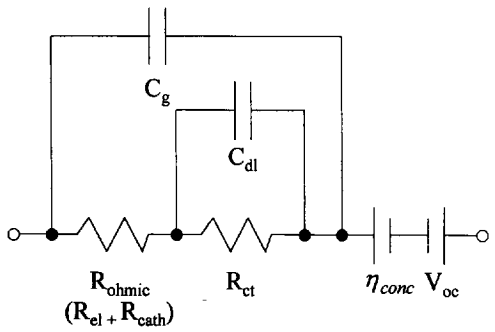

Fig. 7. Equivalent circuit model for the lithium/iodine battery.

4.6. Comparison of model to pulse data

When developing equivalent-circuit models for batteries, it is imperative that the models be verified for the particular range of applications. In this case, for example, it is necessary to determine if the use of ideal circuit elements to represent the observed impedance behavior is an acceptable approximation. Additionally, it must be shown that ignoring the time dependence of concentration polarization does not introduce a significant error on the time scale of interest. One comparison of the model to impedance and pulse data is shown in Figs. 8–10.

Fig. 8 compares a complex-plane plot of a measured impedance spectrum to a corresponding impedance spectrum simulated with ideal circuit elements. Fig. 9(a) and (b) shows the same information on a Bode diagram. While the differences in the complex-plane plot are striking, inspection of the Bode diagram shows that much of the difference lies in the measured versus calculated phase shift at certain frequencies. The corresponding differences in the magnitude of the measured and simulated impedance are relatively small.

The conformance of predicted pulse behavior to observed behavior is explored in Fig. 10(a), (b) and (c). These data were collected during the application of a 50 mA pulse to the battery. Fig. 10(a) shows the excellent agreement between the model and the observed behavior at short time frames. At

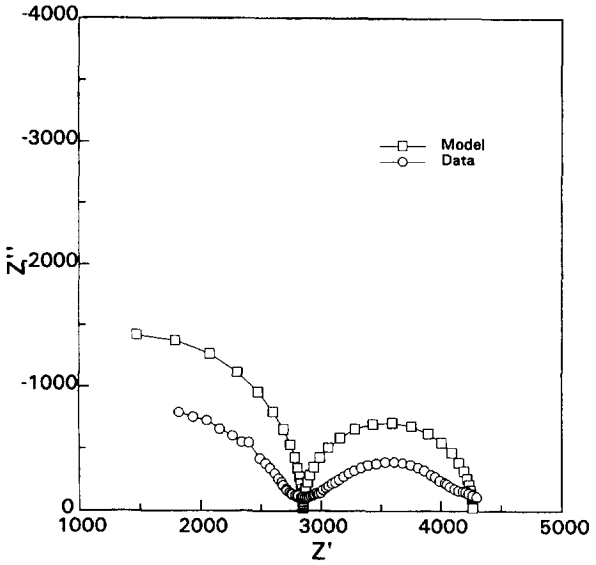

Fig. 8. Comparison of measured and simulated impedance spectra in the complex-plane.

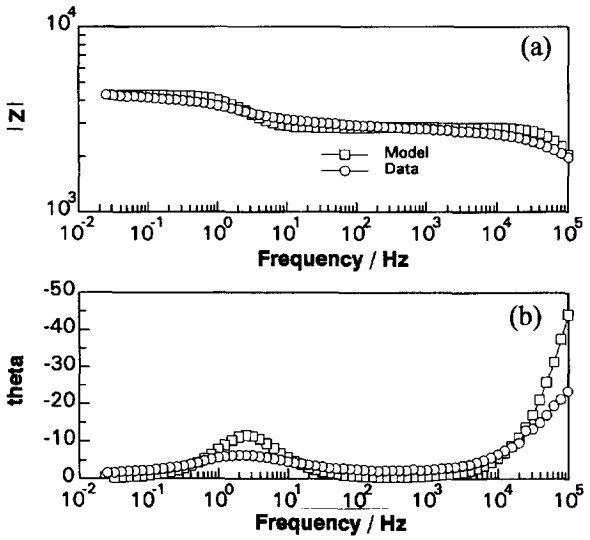

Fig. 9. Comparison of measured and simulated impedance magnitude (a) and phase angle (b).

slightly longer times (Fig. 10(b)), the model predicts a slightly lower voltage than is actually observed. This slight difference arises from the use of an ideal capacitor in the equivalent-circuit model. At still longer times (Fig. 10(c)), the observed voltage drops below the predicted voltage.

This demonstrates the onset of concentration polarization which is not treated as a time-dependent quantity in the equivalent-circuit model.

Overall, there is reasonably good agreement between the observed and predicted behavior over a time period of about 100 s. At significantly longer times, the constant-current model described in Ref. [4] becomes applicable. Thus, by a combination of these two models it is possible to predict the load voltage of new battery designs as a function of discharge capacity over a wide range of constant-current and transient conditions. Furthermore, it is possible to estimate performance distributions in the transient model in a manner similar to that we have described for the constant-current case. The performance variation measured in the cells in this study provides an excellent description of the distribution functions

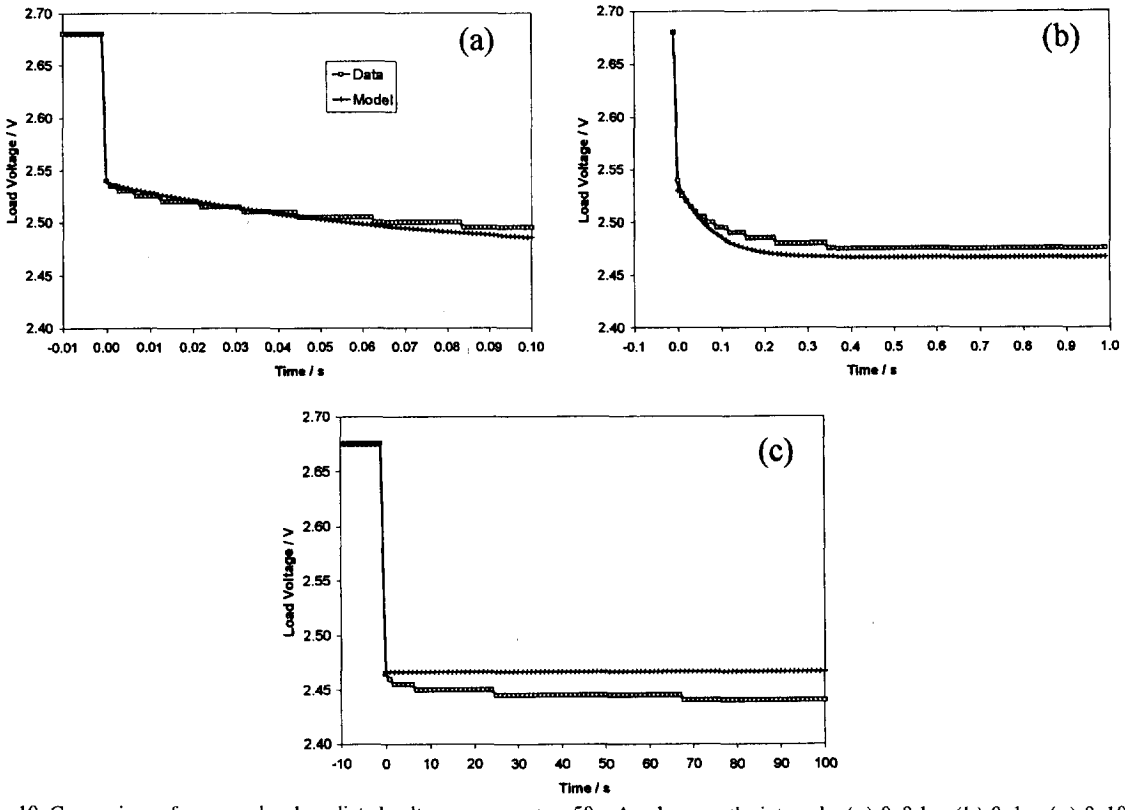

Fig. 10. Comparison of measured and predicted voltage response to a 50 mA pulse over the intervals: (a) 0–0.1 s; (b) 0–1 s; (c) 0–100 s.

for each of the equivalent-circuit elements. This information can be used in Monte Carlo simulations to extend the model to estimate performance distributions for new cell designs.

References

[1] P. Skarstad, A. Crespi, C. Schmidt and D. Untereker, in A. Attewell and T. Keily (eds.), *Power Sources 15*, International Power Sources Committee, Crowborough, UK, 1995, p. 167.

[2] C. Schmidt and P. Skarstad, in K. Abraham and M. Salomon (eds.), *Proc. Symp. Primary and Secondary Lithium Batteries*, Vol. 91-3, The Electrochemical Society, Inc., Princeton, NJ, 1991, p. 75.

[3] P. Skarstad and C. Schmidt, in K. Abraham and M. Salomon (eds.), *Proc. Symp. Primary and Secondary Lithium Batteries*, Vol. 91-3, The Electrochemical Society, Inc., Princeton, NJ, 1991, p. 85.

[4] C. Schmidt and P. Skarstad, in T. Keily and B.W. Baxter (eds.), *Power Sources 13*, International Power Sources Committee, Crowborough, UK, 1991, p. 347.

[5] C. Holmes, in B.B. Owens (ed.), *Batteries for Implantable Biomedical Devices*, Plenum, New York, 1986, p. 139.

[6] G. Phillips and D. Untereker, in B.B. Owens and N. Margalit (eds.), *Proc. Symp. Power Sources for Biomedical Implantable Applications and Ambient Temperature Lithium Batteries*, Vol. 80-4, The Electrochemical Society, Inc., Princeton, NJ, 1980, p. 195.

[7] J. Phipps, T. Hayes, P. Skarstad and D. Untereker, *Solid State Ionics, 18–19* (1986) 1073.